Progress In Electromagnetics Research C, Vol. 131, 159–169, 2023

An Enhanced Active Disturbance Rejection Control of BPMSM Based on Neural Network Parameters Dynamic Adjustment Method

Xin Wang and Huangqiu Zhu*

Abstract—An enhanced linear active disturbance rejection control (E-LADRC) method with dynamically adjust is proposed to improve the observer gain and observation effect in the convenient linear active disturbance rejection control (C-LADRC), reduce the sensitivity of the observer to interference, and find the appropriate observer gain coefficient. Firstly, the mathematical model of bearingless permanent magnet synchronous motor (BPMSM) and the C-LADRC algorithm are described and analyzed. Secondly, the E-LADRC algorithm is designed to overcome the shortcomings of the C-LADRC. Thirdly, the back propagation neural network (BPNN) algorithm with strong self-learning and adaptive ability is used to dynamically adjust the parameters of the E-LADRC, so as to improve the performance of the control system. Finally, the whole control system is analyzed, and the effectiveness of the proposed algorithm is verified on the experimental platform. The experimental results show that the proposed control algorithm can effectively reduce the jitter amplitude of speed and displacement.

1. INTRODUCTION

Bearingless permanent magnet synchronous motor (BPMSM) combines the magnetic bearing technology with permanent magnet synchronous motor and controls the suspension and rotation of the rotor through the stator windings of the motor. Since the transmission shaft is not in contact with the stator, BPMSM has the characteristics of no mechanical friction and wear, high critical speed, maintenance free, long life, and no pollution [1, 2]. Since the BPMSM superimposes torque magnetic field and suspension magnetic field, the whole system will be a high-order, multivariable, and strong coupling nonlinear system. Therefore, the classical proportional integral differential (PID) control will not meet the high performance control requirements of the BPMSM [3]. In order to make the BPMSM have high-performance control effects, many control methods have been applied, such as sliding mode control [4], internal model control [5], neural network control [5], and active disturbance rejection control (ADRC) [3, 6–9]. Because sliding mode control method, internal model control method and neural network control method have poor parameter sensitivity, it is difficult to replace the PID control. The ADRC is independent of the actual model and can use the extended state observer to compensate the total disturbance in real-time, so as to achieve high performance control effect.

In previous studies, several scholars use ADRC to achieve high-performance control of bearingless motors. In [3], cascaded extended state observers (ESOs) are used to realize the ADRC control of speed and displacement, which improve the dynamic performance and control accuracy of the whole control system. In [6], fuzzy neural network inverse system and the ADRC method are used to realize the high-performance decoupling control of the BPMSM. Although the performance of the control system is better than that of the PID method, the entire algorithm requires too much computation. In [7], the corresponding ESO and state error feedback (SEF) are designed based on the derived displacement

Received 21 February 2023, Accepted 16 March 2023, Scheduled 25 March 2023
* Corresponding author: Huangqiu Zhu (zhuhuangqiu@ujs.edu.cn).
The authors are with the School of Electrical and Information Engineering, Jiangsu University, Zhenjiang 212013, China.

and rotational speed integral series standard mathematical model of the single-winding flux-switching bearingless motor as the basis of the ADRC. At the same time, the adjustment process of the parameters is analyzed by combining the parameters with the bandwidth.

A single constant parameter cannot affect the performance of the ADRC control method, despite its strong control performance. Da Silva et al. (2021) regard the error and the incremental change of the ADRC parameters as the input and output signals of the fuzzy control algorithm respectively to realize the dynamic adjustment of parameters [8]. However, fuzzy control relies on strong expert experience, and poor fuzzy control experience will reduce the performance of the entire control system. In [9], the particle swarm genetic algorithm is used in a bearingless induction motor to optimize the parameters of the ADRC, which greatly improves the performance of the control system. The real-time performance of this approach, however, is challenging to satisfy because it is created with 10 populations and 100 iterations. Similarly, other intelligent optimization algorithms can also optimize the ADRC parameters. Although the optimized parameters can improve the performance of the control system, the real-time performance of the system is difficult to be satisfied [10, 11]. Although the aforementioned papers can enhance the performance of the control system by dynamically adjusting the ADRC parameters, there are more or less drawbacks. Therefore, it is necessary to continue researching the dynamic adjustment of the ADRC parameters.

The rest of this paper is structured as follows. In Section 2, the mathematical model of the BPMSM and the algorithm structure of the ADRC are derived. In Section 3, the E-LADRC algorithm is designed to overcome the shortcomings of the C-LADRC. In Section 4, the process of dynamic parameter adjustment of the BPNN algorithm is analyzed and deduced in detail. Section 5 proves the feasibility of this method through experiments. The content of this paper is summarized in Section 6.

2. THE BPMSM MATHEMATICAL MODEL AND ADRC ALGORITHM

2.1. The BPMSM Mathematical Model

The torque windings and suspension force windings of the BPMSM are placed in stator slots, and the schematic diagram of the BPMSM is shown in Fig. 1. When the pole pairs of the torque windings P_M and the suspension force windings P_B differ by 1, and the current frequency connected to the two sets of windings is equal, i.e., $P_M = P_B \pm 1$, $\omega_M = \omega_B$, BPMSM will be able to stabilize suspension. At this time, the corresponding expression of the suspension force in the control system is

$$\begin{cases} \Sigma F_x = F_{ux} + F_{dx} - F_x = m\ddot{x} \\ \Sigma F_y = F_{uy} + F_{dy} - F_y = m\ddot{y} \end{cases} \tag{1}$$

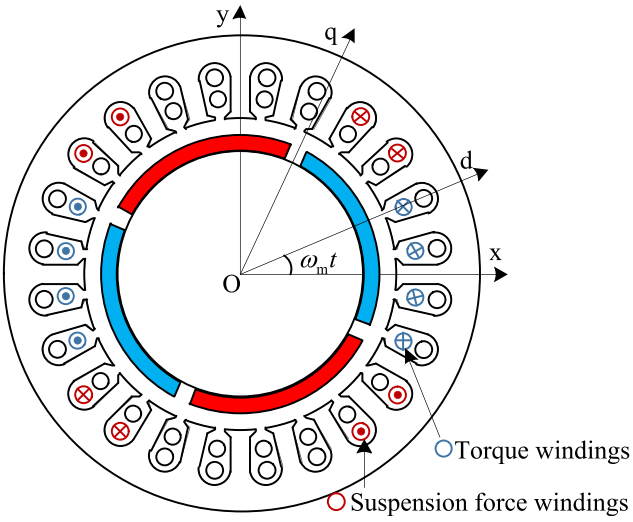

Figure 1. Schematic diagram of the BPMSM.

where F_{ux} and F_{uy} are unbalanced magnetic pull in x- and y-axis static coordinate systems, respectively. F_{dx} and F_{dy} are the additional disturbing forces in the x- and y-axis directions, respectively. F_x and F_y are respectively the controllable suspension force in the x- and y-axis directions.

The expressions of electromagnetic torque and mechanical motion equation are

$$T_e = 1.5P_M\lambda_f i_{Mq} + M'd\left(I_f i_{Bq} + i_{Mq} i_{Bd}\right) + M'q\left(I_f i_{Bd} - i_{Mq} i_{Bq}\right) \tag{2}$$

$$J\frac{\mathrm{d}\omega_m}{\mathrm{d}t} = T_e - T_L - B\omega_m \tag{3}$$

where P_M is the number of motor pole pairs, λ_f the permanent magnet flux linkage, J the moment of inertia, ω_m the mechanical angular speed of the motor, T_L the load torque, B viscous damping. I_f is the equivalent excitation current amplitude of the permanent magnet. i_{Md} and i_{Mq} are currents of d- and q-axes at motor-side, respectively. M' is the mutual inductance coefficient. d and q are the displacements of d- and q-axes, respectively.

2.2. Establishment of the Conventional LADRC Control Algorithm

The high-performance control requirements of the BPMSM cannot be met by a standard PID control since there are several coupling considerations involved in its operation. The ADRC achieves high performance control effect by actively observing the total disturbance of the system and actively suppressing the disturbance. Therefore, ADRCs are used to replace the PID controllers of the BPMSM speed loop and displacement loop [12, 13]. At the same time, in order to ensure the rapidity of current loop, PI controllers are still used for current loop at motor side and suspension side.

2.2.1. C-LADRC Design of Motor-side Speed Loop

According to the previous expression of electromagnetic torque and mechanical motion equation, the following expression can be constructed.

$$\begin{aligned}\frac{\mathrm{d}\omega_M}{\mathrm{d}t} &= \frac{1.5P_M^2\lambda_f}{J} i_{Mq} + \frac{1}{J}\left[M'dP_M\left(I_f i_{Bq} + i_{Mq} i_{Bd}\right) + M'qP_M\left(I_f i_{Bd} - i_{Mq} i_{Bq}\right) - P_M T_L - B\omega_M\right] \\ &= bu + f_w\end{aligned} \tag{4}$$

where b is the motor parameter gain, $b = \frac{1.5P_M^2\lambda_f}{J}$, and f_w is the total disturbance.

According to the above formula, the form of (6) conforms to the normal form of the ADRC; therefore, the ADRC can be used to control the speed. The ADRC of the motor-side speed loop shown in Fig. 2(a) can be constructed.

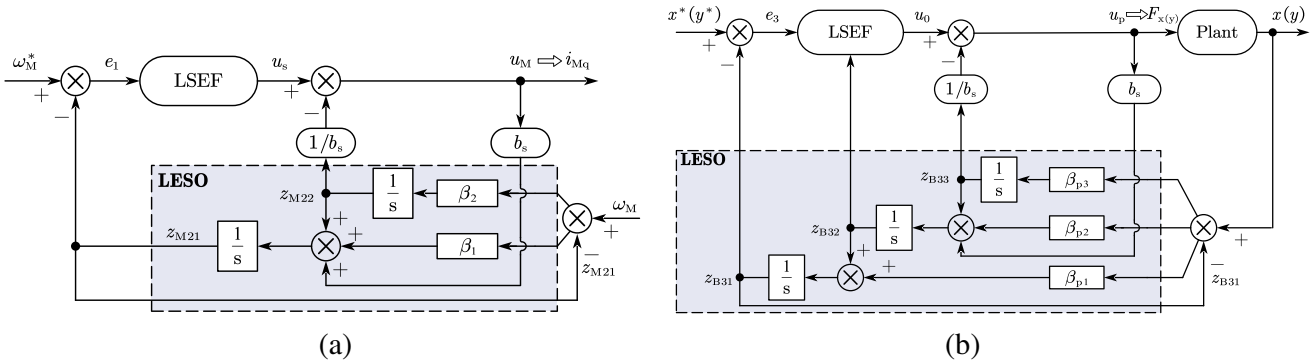

Figure 2. Block diagram of LADRC. (a) Speed loop. (b) Displacement loop.

The state equation in the linear ESO (LESO) can be written as

$$\begin{cases}\dot{z}_{M21} = z_{M22} - \beta_1\left(z_{M21} - \omega_M\right) + b_s u_M \\ \dot{z}_{M22} = -\beta_2\left(z_{M21} - \omega_M\right)\end{cases} \tag{5}$$

where z_{M21} and z_{M22} are the speed observation value and disturbance observation value, respectively. β_1 and β_2 are the observer gains.

The equation in linear SEF (LSEF) can be written as

$$u_s = \beta_3 \left(\omega_M^* - z_{M21}\right) \tag{6}$$

where ω_M^* is the given value of motor speed, β_3 the gain of LSEF, and u_s the LSEF output value.

The compensation output of the disturbance is

$$u_M = u_s - \frac{z_{M22}}{b_s} \tag{7}$$

2.2.2. C-LADRC Design of Suspension-Side Displacement Loop

The ADRC structure of the suspension-side displacement loop is similar to that of the motor-side speed loop. According to (1), the form of the active disturbance rejection normal form can be constructed.

$$\begin{cases} \ddot{x} = -\dfrac{1}{m}F_x + \dfrac{1}{m}\left(F_{ux} + F_{dx}\right) = \dfrac{1}{m}F_x + \dfrac{1}{m}\left(F_{ux} + F_{dx} - 2F_x\right) = b_1 u + f_{x1} \\ \ddot{y} = -\dfrac{1}{m}F_y + \dfrac{1}{m}\left(F_{uy} + F_{dy}\right) = \dfrac{1}{m}F_y + \dfrac{1}{m}\left(F_{uy} + F_{dy} - 2F_y\right) = b_1 u + f_{y1} \end{cases} \tag{8}$$

where f_{x1} and f_{y1} are the disturbance values.

According to (8), the ADRC of the suspension-side displacement loop shown in Fig. 2(b) can be constructed according to the corresponding normal form.

Taking the ADRC in the x axis direction as an example, the state equation inside the LESO can be written as

$$\begin{cases} \dot{z}_{B31} = z_{B32} - \beta_{p1}\left(z_{B31} - x\right) \\ \dot{z}_{B32} = z_{B33} - \beta_{p2}\left(z_{B31} - x\right) + b_p u_p \\ \dot{z}_{B33} = -\beta_{p3}\left(z_{B31} - x\right) \end{cases} \tag{9}$$

where z_{B31} is the displacement observation value; z_{B32} is the observed value of displacement differential; z_{B33} is the disturbance value; β_{p1}, β_{p2}, and β_{p3} are the gain of observer.

The equation in LSEF can be written as

$$u_0 = \beta_{p4}\left(x - z_{B31}\right) - \beta_{p5} z_{B32} \tag{10}$$

where β_{p4} and β_{p5} are the gain of the LSEF.

The compensation output of the disturbance is

$$u_p = u_0 - \frac{z_{B33}}{b_p} \tag{11}$$

The C-LADRC of motor-side speed loop and suspension-side displacement loop both need high bandwidth to meet the requirements of fast tracking. However, low anti-interference capacity of the system will result from high bandwidth, which makes it difficult to find the parameters of the control system. Therefore, an E-LADRC is designed based on LADRC to overcome the defects of the LADRC and improve the disturbance immunity and stability of the system.

3. DESIGN OF THE E-LADRC CONTROLLERS

3.1. E-LADRC Design of Motor-Side Speed Loop

The following improvements are made based on Section 2.2.1. A cascaded LESO is used to replace the traditional LESO. The schematic is shown in Fig. 3. The overall disturbance of the LESO1 is considered as the known disturbance of the LESO2, and this disturbance will be used as the input of the LESO2. The LESO2 observes the remaining disturbances except z_{M22}. By adding the estimated interference of LESO1 and LESO2, the overall interference of the torque system is removed. The detailed analysis is described below.

The state equation of LESO1 is established as

$$\begin{cases} \dot{z}_{M21} = z_{M22} - \beta_{w1}(z_{M21} - \omega_M) + b_s u_M \\ \dot{z}_{M22} = -\beta_{w2}(z_{M21} - \omega_M) \end{cases} \tag{12}$$

The preliminary estimated disturbance of the LESO1 is z_{M22}, which is regarded as the known part of the LESO2. The state equation of the LESO2 is established as

$$\begin{cases} \dot{s}_{M21} = s_{M22} + z_{M22} - \beta_{w3}(s_{M21} - \omega_M) + b_s u_M \\ \dot{s}_{M22} = -\beta_{w4}(s_{M21} - \omega_M) \end{cases} \tag{13}$$

where the tracking effect on speed for s_{M21} is comparable to that for z_{M21}. s_{M22} is the observed value of the remaining disturbance.

In light of the analysis above, the enhanced LESO can be used in place of the conventional LESO as an integrator. The enhanced LESO improves stability of the speed loop by reducing the weight of observation compared to the conventional LESO, allowing the disturbance to be tracked and corrected timely with a small observer bandwidth. In Fig. 3(a), the measured speed is chosen because LESO1 and LESO2 have slow observation speeds, and the chosen observer bandwidth is quite small. In order to simplify the complexity of parameters adjustment, the parameters are set as $[\beta_{w1} \quad \beta_{w2}] = [\beta_{w3} \quad \beta_{w4}]$.

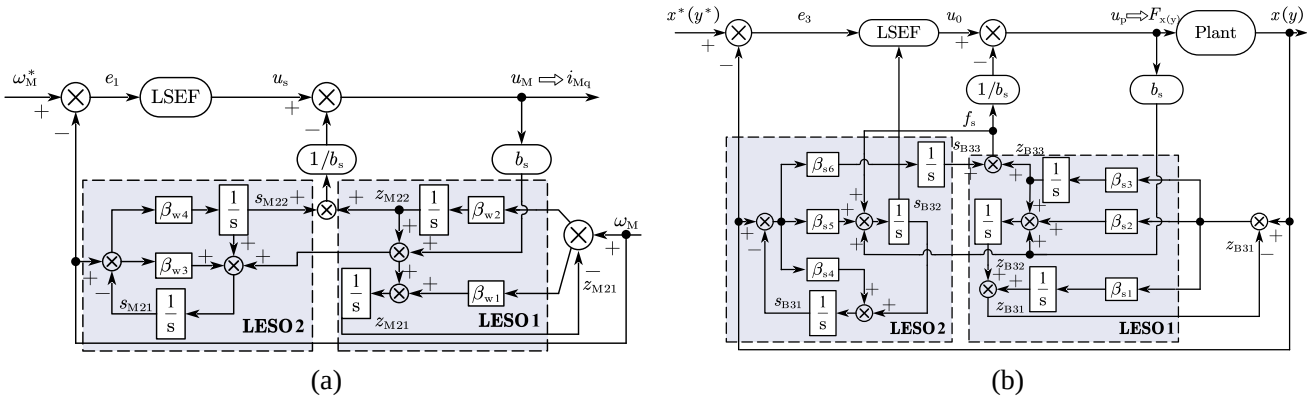

Figure 3. Block diagram of speed loop E-LADRC. (a) Speed loop. (b) Displacement loop.

3.2. E-LADRC Design of Suspension-Side Displacement Loop

The state equation of the LESO1 in Fig. 3(b) is established as

$$\begin{cases} \dot{z}_{B31} = z_{B32} - \beta_{s1}(z_{B31} - x) \\ \dot{z}_{B32} = z_{B33} - \beta_{s2}(z_{B31} - x) + b_p u_p \\ \dot{z}_{B33} = -\beta_{s3}(z_{B31} - x) \end{cases} \tag{14}$$

The preliminary observed disturbance of the LESO1 is z_{B33}. The state equation of the LESO2 is

$$\begin{cases} \dot{s}_{B31} = s_{B32} - \beta_{s4}(s_{B31} - x) \\ \dot{s}_{B32} = s_{B33} + z_{B33} - \beta_{s5}(s_{B31} - x) + b_p u_p \\ \dot{s}_{B33} = -\beta_{s6}(s_{B31} - x) \end{cases} \tag{15}$$

where s_{B31} and s_{B32} have a similar tracking effect on speed to z_{B31} and z_{B32}. s_{B33} is the observed value of the remaining disturbance.

Similarly, the third-order E-LESO can be regarded as the double integral series. The E-LESO boosts the observer's tracking capabilities in comparison to the C-LESO. When a high observer bandwidth is selected, the anti-interference ability of the suspension system will be improved, because the system can still maintain stability. In order to simplify the complexity of parameters adjustment, the parameters are set as $[\beta_{s1} \quad \beta_{s2} \quad \beta_{s3}] = [\beta_{s4} \quad \beta_{s5} \quad \beta_{s6}]$.

In [3], the adjustment of controller parameters mentioned above is related to the bandwidth parameters, which can effectively reduce the difficulty of parameter adjustment. However, the bandwidth parameters require strong practical adjustment experience, and a set of parameters cannot be universal. Therefore, the adjustment of parameters is difficult.

4. THE BPNN ALGORITHM AND ANALYSIS

Since many gains and coefficients in the E-LADRC have a crucial impact on the operation of the BPMSM, dynamic adjustment of these gains and coefficients can effectively improve the operation quality of the motor. The BPNN algorithm is a multilayer feedforward neural network trained according to the error back propagation algorithm, which includes input layer, hidden layer, and output layer. The BPNN will not have a great impact on the global training results when its local or partial neurons are damaged. In addition, the BPNN can greatly reduce the computation time because of its computational advantages compared with evolutionary algorithm. The specific algorithm block diagram for adjusting BPNN E-LADRC parameters is shown in Fig. 4(a).

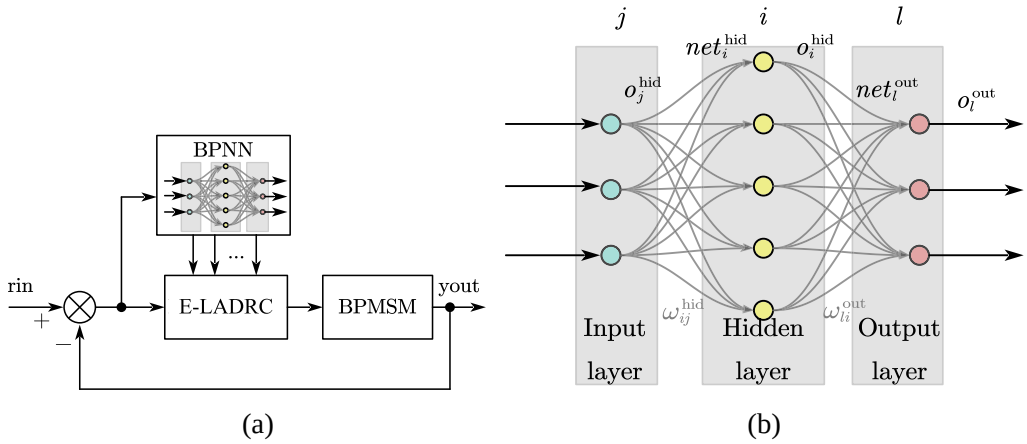

Figure 4. Block diagram of E-LADRC and BPNN. (a) E-LADRC. (b) BPNN.

In this paper, a three-layer BPNN is used. The input layer selects the important three variables in the neural network algorithm, error e, actual output component y, and constant item 1. The number of hidden layer nodes is determined to be 5 based on the comprehensive control effect and calculation amount. The output of the output layer corresponds to the gains of the LESO1 and LESO2 of the speed loop E-LADRC controller β_{w1}, β_{w2}, β_{w3}, β_{w4}, and correlation coefficient b_s. The output layer of BPNN in suspension control corresponds to the gains of the LESO1 and LESO2 of displacement loop E-LADRC controller β_{s1}, β_{s2}, β_{s3}, β_{s4}, β_{s5}, β_{s6}, and correlation coefficient b_p. The basic structure of the designed BPNN is shown in Fig. 4(b).

Take the structure in Fig. 4(b) as an example to analyze the network. The input and output parts corresponding to the hidden layer are

$$\begin{cases} \text{net}_i^{\text{hid}}(k) = \sum_{j=1}^{3} w_{ij}^{\text{hid}} o_j^{\text{in}} \\ o_i^{\text{hid}}(k) = f\left(\text{net}_i^{\text{hid}}(k)\right) \end{cases}, \quad i = 1, 2, ..., 5 \tag{16}$$

where w_{ij}^{hid} is the weight coefficient of the hidden layer.

The input and output parts of the output layer are

$$\begin{cases} \text{net}_l^{\text{out}}(k) = \sum_{i=1}^{5} w_{li}^{\text{out}} o_i^{\text{im}}(k) \\ o_l^{\text{out}}(k) = g\left(\text{net}_l^{\text{out}}(k)\right) \end{cases}, \quad l = 1, 2, 3 \tag{17}$$

The parameters of the E-LADRC that need to be adjusted by the BPNN are represented by each element of the output node. (16) and (17) employ the following functions, respectively, as the activation functions $f(\cdot)$ and $g(\cdot)$, where $f(x) = (e^x - e^{-x})/(e^x + e^{-x})$, $g(x) = (e^x)/(e^x + e^{-x})$.

The performance evaluation function is defined as

$$E(k) = \frac{1}{2}[\text{rin}(k) - \text{yout}(k)]^2 \tag{18}$$

The formula can be updated continuously by using the gradient descent method, that is, search and adjust according to the negative gradient direction of $E(k)$ to the weight coefficients.

The updating process of the parameters of the accelerated gradient descent method is

$$\Delta w_{li}^{\text{out}}(k) = -\eta \left[(1-\mu) \frac{\partial E(k)}{\partial w_{li}^{\text{out}}(k)} + \mu \frac{\partial E(k-1)}{\partial w_{li}^{\text{out}}(k-1)} \right] \tag{19}$$

where η is the learning rate, and μ is the momentum factor.

The weight calculation process of the output layer is

$$h(k) = \frac{\partial E(k)}{\partial w_{li}^{\text{out}}(k)} = \frac{\partial E(k)}{\partial y(k)} \cdot \frac{\partial y(k)}{\partial o_l^{\text{out}}(k)} \cdot \frac{\partial o_l^{\text{out}}(k)}{\partial \text{net}_l^{\text{out}}(k)} \cdot \frac{\partial \text{net}_l^{\text{out}}(k)}{\partial w_{li}^{\text{out}}(k)} \tag{20}$$

Since the second term in (20) is unknowable and hard to calculate, and the following formulation can be used in its place.

$$\frac{\partial y(k)}{\partial o_l^{\text{out}}(k)} \to \text{sgn}\left(\frac{\partial y(k)}{\partial \Delta o_l^{\text{out}}(k)} \right) \tag{21}$$

The third and fourth terms on the right side of (20) can be expressed as

$$\frac{\partial o_l^{\text{out}}(k)}{\partial \text{net}_l^{\text{out}}(k)} \cdot \frac{\partial \text{net}_l^{\text{out}}(k)}{\partial w_{li}^{\text{out}}(k)} = g'\left(\text{net}_l^{\text{out}}(k)\right) \cdot o_i^{\text{hid}}(k) \tag{22}$$

where $g'(\cdot) = g(\cdot)(1 - g(\cdot))$.

The following formula is derived by substituting (20)–(22) into (19).

$$\Delta w_{li}^{\text{out}}(k) = -\eta \left[(1-\mu)\, \delta_l^{\text{out}}(k)\, o_i^{\text{hid}}(k) + \mu \delta_l^{\text{out}}(k-1)\, o_i^{\text{hid}}(k-1) \right] \tag{23}$$

where $\delta_l^{\text{out}}(k) = -e(k) \cdot \text{sgn}\left(\frac{\partial y(k)}{\partial \Delta o_l^{\text{out}}(k)} \right) \cdot g'(net_l^{\text{out}}(k))$.

Similarly, the weight update formula of the input layer is

$$\Delta w_{ij}^{\text{hid}}(k) = -\eta \left[(1-\mu)\, \delta_i^{\text{hid}}(k)\, o_j^{\text{hid}}(k) + \mu \delta_i^{\text{hid}}(k-1)\, o_j^{\text{hid}}(k-1) \right] \tag{24}$$

where $\delta_i^{\text{hid}}(k) = \delta_l^{\text{out}}(k) \cdot w_{li}^{\text{out}}(k) \cdot f'(\text{net}_l^{\text{out}})$, $f'(\cdot) = (1 - f(\cdot))/2$.

The adaptive learning rate is utilized to enhance the optimization performance of the BPNN by accelerating training and preventing the network from reaching the local minimum. The following form can be used to iteratively update the specific learning rate.

$$\eta(k) = 2^{\text{sgn}(h(k) \cdot h(k-1))} \eta(k-1) \tag{25}$$

In this paper, the BPNN is used to continuously update the E-LADRC parameters to improve the performance of the control system. The general block diagram of the BPMSM control system based on the BPNN E-LADRC is shown in Fig. 5. The whole control is divided into suspension vector control and motor vector control. Between them, the proposed algorithm is used to update the parameters of the displacement loop E-LADRC in suspension vector control and the speed loop E-LADRC in motor vector control. Since the current loop in suspension vector control and motor vector control can be equivalent with a first-order link, a simple and efficient PI controller can be used. As a result, the BPNN algorithm better meets performance requirements when real-time requirements are high. The BPNN in the speed loop takes the speed error and actual speed as the input of the module. After real-time adjustment, it outputs 4 gains and correlation coefficients in (12)–(13). The BPNN in the displacement loop takes displacement error and actual displacement as the input of the module. After real-time adjustment, it outputs 6 gains and 1 correlation coefficient in (14)–(15).

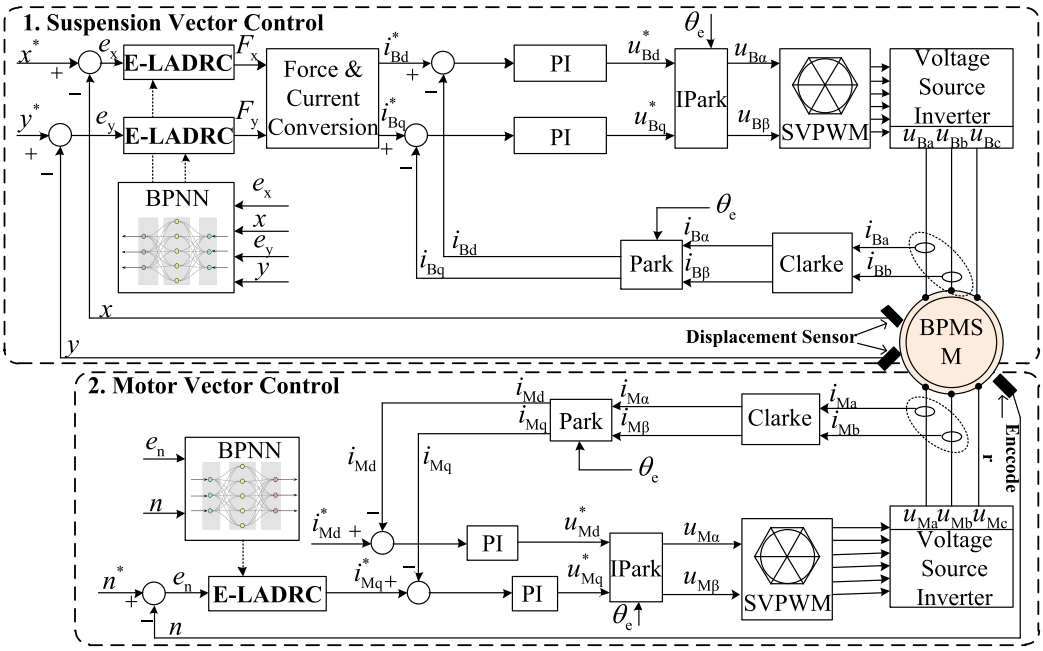

Figure 5. The general block diagram of the BPMSM control system.

5. EXPERIMENTAL ANALYSIS

In order to verify the effectiveness of the proposed BPNN E-LADRC algorithm applied to the BPMSM, the corresponding experiments are carried out on the experimental platform. The experimental prototype platform and specific parameters are shown in Fig. 6 and Table 1. In Fig. 6, the upper power drive circuit board supplies power to the torque windings of the BPMSM, and the lower power drive circuit board supplies power to the suspension force windings of the BPMSM. The initial parameters of the speed loop C-LADRC in Section 2.2.1 are set as $\beta_1 = 2.5e5$, $\beta_2 = 2e3$, $\beta_3 = 40$, $b_s = 166$. The initial parameters of the displacement loop C-LADRC in Section 2.2.2 are set as $\beta_{p1} = 8e3$, $\beta_{p2} = 1.2e3$, $\beta_{p3} = 60$, $\beta_{p4} = 15$, $\beta_{p5} = 8e-3$, $b_p = 6.25$. The PI parameters of the current loop at the motor-side are respectively set to $K_p = 0.23$, $K_i = 1.7\text{e}-2$. The PI parameters of the current loop at the suspension-side are respectively set to $K_p = 0.5$, $K_i = 4.5\text{e}-3$.

Since the BPNN does not need to update parameters in every control cycle, the execution frequency

Symbol	Value	Symbol	Value
U_N (V)	220	n_N (r/min)	3000
P_N (kW)	1.1	P_M/P_B	1/2
λ_f (Wb)	0.166	M'	6.67
R_M (Ω)	2.32	R_B (Ω)	1.85
L_M (mH)	13.42	L_B (mH)	2.34

Table 1. The parameters of the prototype.

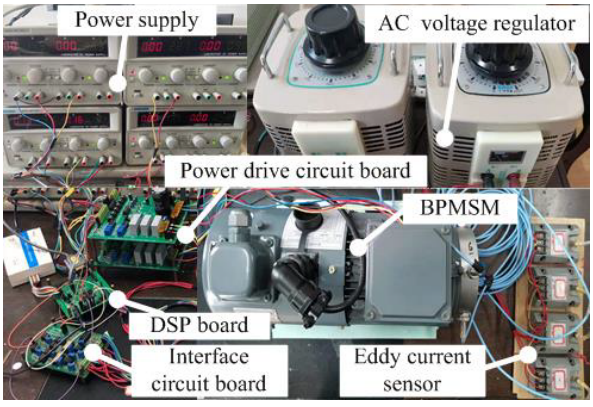

Figure 6. Experimental platform.

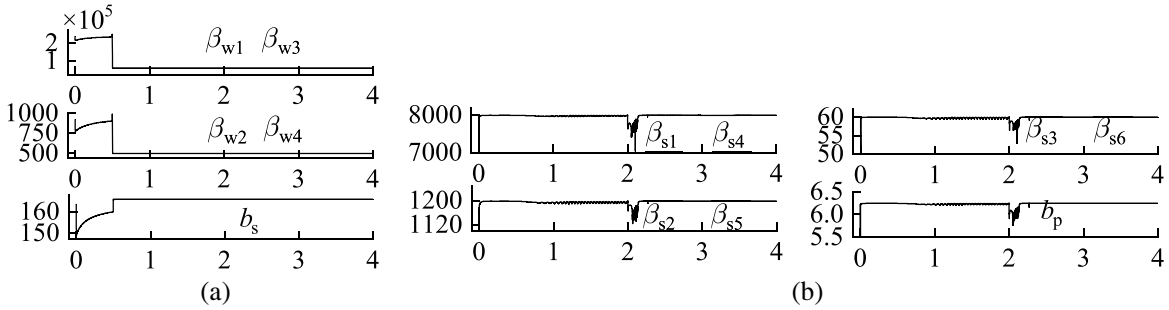

Figure 7. ADRC parameter adjustment process. (a) Motor-side. (b) Suspension-side.

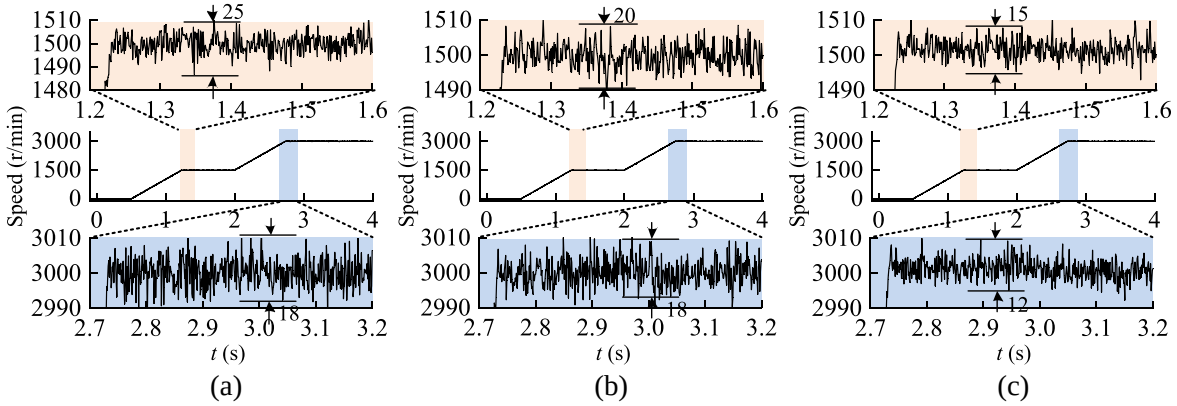

Figure 8. Speed waveforms in different methods. (a) C-LADRC. (b) BPNN C-LADRC. (c) E-LADRC.

of the BPNN can be appropriately reduced. Here, the number of BPNN executions is set to one tenth of the interrupt frequency. The process of BPNN adjusting the E-LADRC parameters in real-time is shown in Fig. 7.

Figure 8 shows the speed waveforms of three different control algorithms. Fig. 8(a) is the speed waveform of the C-LADRC algorithm. At 1500 r/min, the speed changes by 25 r/min, and at 3000 r/min, it changes by 18 r/min. Fig. 8(b) shows the speed waveform of C-LADRC parameters dynamically adjusted by BPNN. At 1500 r/min, the speed changes by 20 r/min, and at 3000 r/min, it changes by 18 r/min. Fig. 8(c) shows the speed waveform of the proposed algorithm. At 1500 r/min, the speed changes by 15 r/min. Compared with C-LADRC, the speed change is reduced by 40%, and compared with BPNN C-LADRC, the speed change is reduced by 25%. At 3000 r/min, the speed changes by 12 r/min. Compared with C-LADRC, the speed change is reduced by 33.3%, and compared with BPNN C-LADRC, the speed change is reduced by 33.3%. The speed fluctuation of the proposed algorithm is smaller than that of the previous two algorithms.

Figure 9 shows the displacement waveforms of three different control algorithms. Fig. 9(a) is the displacement waveform of the C-LADRC algorithm. At 2 s, the displacement in the x direction changes suddenly and stabilizes at 20 μm after 0.25 s. Fig. 9(b) shows the displacement waveform of C-LADRC parameters dynamically adjusted by BPNN. It can be seen from the figure that within the time range of 0–2 s, the displacement in the x direction and y direction has multiple mutations, which is caused by the instability of parameters during the dynamic adjustment of parameters. At 2 s, the displacement in x direction has sudden changes and is stable at 20 μm after 0.15 s. Fig. 9(c) shows the displacement waveform of the proposed algorithm. It can be seen from the figure that the fluctuation range of displacement is 20 μm in the time range of 0–2 s, and the displacement in the x direction changes abruptly in 2 s and is stable at 20 μm after 0.13 s. The proposed algorithm not only suppresses mutation better, but also has better stability.

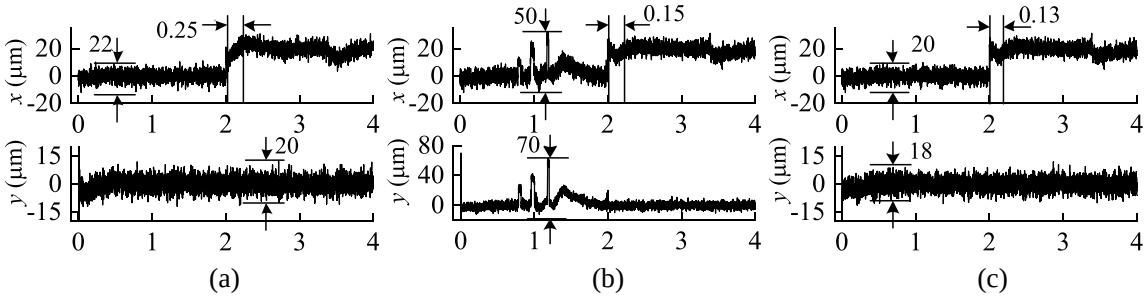

Figure 9. Displacement waveforms in different methods. (a) C-LADRC. (b) BPNN C-LADRC. (c) E-LADRC.

6. CONCLUSION

In this paper, an E-LADRC algorithm based on BPNN parameter dynamic adjustment is proposed to solve the problem of insufficient disturbance rejection at C-LADRC. The E-LADRC algorithm uses two ESOs to replace the ESO in C-LADRC, thus effectively improving the performance of the entire control system. The BPNN method is used to dynamically alter the parameters of E-LADRC in order to address the problem of parameter adjustment. The results of the experiments demonstrate that the algorithm of BPNN dynamic optimization of E-LADRC parameters may significantly enhance control performance, decrease speed and displacement fluctuation, and reduce dynamic response time.

ACKNOWLEDGMENT

This work was supported by the National Natural Science Foundation of China (61973144) and the Postgraduate Research & Practice Innovation Program of Jiangsu Province (KYCX22_3655).

REFERENCES

1. Valente, G., A. Formentini, L. Papini, et al., "Performance improvement of bearingless multisector PMSM with optimal robust position control," *IEEE Transactions on Power Electronics*, Vol. 34, No. 4, 3575–3585, Apr. 2019.
2. Zhu, T., X. Cao, Q. Yu, et al., "Direct torque control with phase commutation optimization for single-winding bearingless switched reluctance motor," *IEEE Transactions on Power Electronics*, Vol. 37, No. 11, 13 238–13 249, Nov. 2022.
3. Yang, Z., J. Jia, X. Sun, and T. Xu, "An enhanced linear adrc strategy for a bearingless induction motor," *IEEE Trans. Transp. Electrif.*, Vol. 8, No. 1, 1255–1266, Mar. 2022.
4. Yang, Z., Q. Ding, X. Sun, et al., "Fractional-order sliding mode control for a bearingless induction motor based on improved load torque observer," *J. Franklin Inst.*, Vol. 358, No. 7, 3701–3725, May 2021.
5. Sun, X., L. Chen, H. Jiang, et al., "High performance control for a bearingless permanent-magnet synchronous motor using neural network inverse scheme plus internal model controllers," *IEEE Transactions on Power Electronics*, Vol. 63, No. 6, 3479–3488, Jun. 2016.
6. Zhu, H. and Z. Gu, "Active disturbance rejection control of 5-degree-of-freedom bearingless permanent magnet synchronous motor based on fuzzy neural network inverse system," *ISA Trans.*, Vol. 101, 295–308, Jun. 2020.
7. Chen, Y. and Y. Zhou, "Active disturbance rejection and ripple suppression control strategy with model compensation of single-winding bearingless flux-switching permanent magnet motor," *IEEE Transactions on Power Electronics*, Vol. 69, No. 8, 7708–7719, Aug. 2022.
8. Da Silva, W., A. O. Salazar, P. V. F. Vieira, et al., "Radial position control of a bearingless machine with active disturbance rejection control fuzzy an approach," *ICA-ACCA*, 1–5, Mar. 2021.

9. Yang, Z., C. Lu, X. Sun, et al., "Study on active disturbance rejection control of a bearingless induction motor based on an improved particle swarm optimization-genetic algorithm," *IEEE Trans. Transp. Electrif.*, Vol. 7, No. 2, 694–705, Jun. 2021.
10. Zhou, X., H. Gao, B. Zhao, and L. Zhao, "A GA-based parameters tuning method for an ADRC controller of ISP for aerial remote sensing applications," *ISA Trans.*, Vol. 81, 318–328, Oct. 2018.
11. Wang, Y., S. Fang, and J. Hu, "Active disturbance rejection control based on deep reinforcement learning of PMSM for more electric aircraft," *IEEE Transactions on Power Electronics*, Vol. 38, No. 1, 406–416, Jan. 2023.
12. Lin, P., Z. Wu, K. Liu, and X. Sun, "A class of linear-nonlinear switching active disturbance rejection speed and current controllers for PMSM," *IEEE Transactions on Power Electronics*, Vol. 36, No. 12, 14 366–14 382, Dec. 2021.
13. Qu, L., W. Qiao, and L. Qu, "Active-disturbance-rejection-based sliding-mode current control for permanent-magnet synchronous motors," *IEEE Transactions on Power Electronics*, Vol. 36, No. 1, 751–760, Jan. 2021.